Current Natural Sciences & Engineering
Volume 3, Issue 1, 2026, 954-963

Design and Characterization of 2D $Ti_3C_2T_x$ MXene as an Efficient Electrode Material for Supercapacitor

Mahaveer Singh[1], Bheem Kumar[1], Pushpendra Kumar Meena[1] and Kedar Singh[1]*

[1]School of Physical Sciences, Jawaharlal Nehru University (JNU), New Delhi 110067, India

Received date:08/05/206, Acceptance date: 12/06/2026

DOI: ***http://doi.org/10.63015/8ms-2500.3.1***

Corresponding Author: kedar@mail.jnu.ac.in

Abstract

The increasing demand for effective energy storage devices has enhanced the need of durable electrode materials for supercapacitors. In this work, $Ti_3C_2T_x$ MXene nanosheets was synthesized via HF etching and subsequent delamination to obtain layered 2D nanosheets. The structural and morphological properties were examined using XRD pattern, SEM, and TEM, confirming the successful synthesis of layered structure, while UV–Visible spectroscopy indicated its optical response. The electrochemical performance was evaluated in a three-electrode setup using nickel foil as the current collector substrate. Cyclic voltammetry (CV) and galvanostatic charge–discharge (GCD) measurements show excellent capacitive behaviour, delivering a notable specific capacitance of 535 F g^{-1} at current density of 1 A g^{-1}. Electrochemical impedance spectroscopy (EIS) revealed low R_s and efficient charge transfer kinetics, supporting enhanced electrochemical performance. The superior capacitance is due to the high conductivity, wide surface area, and rapid ion transport within the $Ti_3C_2T_x$ MXene nanosheets, demonstrating that $Ti_3C_2T_x$ is an effective electrode material for high performing supercapacitor application.

Keywords: MXene; $Ti_3C_2T_x$; Supercapacitors; Electrochemical Studies; Energy Storage.

1. Introduction

In growing world, the use of green energy resources has accelerated the development of energy storage devices such as supercapacitor and batteries [1–3]. Supercapacitor are well recognized for high-power density, quick charge discharge capabilities, long term cyclic stability, cost effective, and environment friendly [4–8]. Flexible supercapacitor provides significant benefits over traditional supercapacitor, including lightweight, great flexibility, and compact size making them ideal for portable electronics [9]. Electrodes are critical for tuning the electrochemical performance of supercapacitor. Two-dimensional nanomaterials have gained popularity due to their increased surface area, high electronic conductivity, and mechanical compatibility[10]. As a promising material for supercapacitor application are 2D transition metal dichalcogenides (TMDs) and MXene have been explored due to high surface area and mechanical flexibility [11–15].

Among various electrochemical materials, a family of 2D transition metal carbide/nitrides are promising electrode material for energy storage for owing to their adaptable properties such as high electrical conductivity, electrochemical versatility, large surface area, easy to synthesis, easily accessible tunable morphology, and superficial electrolyte/ion transport through widely interlayered spacing [16–18]. MXene are often obtained from MAX phase, which are which are layered ternary ceramic materials given by the formula $M_{n+1}AX_n$ (n = 1−4), where M is a transition metal like Ti, V, Zr, Mo, Hf, Mo, Nb, etc., A is a group 13 or 14 element, and X is N and/or C. The prepared MXene are denoted as $M_{n+1}XnT_x$, where T_x stands for surface terminations such as F, O, OH, and Cl[19]. $Ti_3C_2T_x$ is the most extensively investigated MXene because of its high stability [20]. However, MXene have some drawbacks, including restacking inclination due to intense hydrogen bonding and weak van der wall interaction, superficial flaws in colloidal solution, and low flexibility, which have limited their current applications [21,22]. The main determinants of high electrochemical performance are the operative methodological characteristics, structural robustness, high electrically conductive, and abundance of active sites. Priyanka et al. achieved capacity of $Ti_3C_2T_x$ in 5 M KOH electrolyte is 368.5 F g^{-1} [23]. Xu et al. found the specific capacitance of $Ti_3C_2T_x$-rGO composite is 154 F g^{-1} at a current density of 2 A g^{-1} in electrolyte 6 M KOH [24].

In present work, $Ti_3C_2T_x$ MXene nanosheets were synthesized by HF-etching method, trailed by exfoliation in LiCl solutions to attain delaminated material. Structural (XRD) and Morphological (SEM and TEM) analysis gives the agreement for successful synthesis if $Ti_3C_3T_x$ sheets. Using a three-electrode setup, the electrochemical performance of pristine $Ti_3C_2T_x$ MXene nanosheets was methodically assessed. The charge-storage and resistance behavior of the electrode material evaluated using thorough electrochemical tests, like cyclic voltammetry (CV), galvanostatic charge–discharge (GCD), and electrochemical impedance spectroscopy (EIS). The active substance was fabricated on nickel foil to create the working electrodes, and 1 M H_2SO_4 electrolyte was used for all electrochemical tests. According to the GCD tests, the $Ti_3C_2T_x$ MXene electrode produced a huge specific capacity of 535 F g^{-1} at a current density of 1 A g^{-1}. Similarly, a specific capacity of 387.5 F g^{-1} was found by CV analysis at scan rate 20 mV s^{-1}. $Ti_3C_2T_x$ MXene nanosheets is distinctive two-dimensional layered design, which provides a huge accessible surface area, superior electronic conductivity, and an abundance of

electro-chemical active sites for effective ion transport and charge transfer, is responsible for the improved electrochemical performance. These results shown for $Ti_3C_2T_x$ MXene is great promise as an electrode material for advanced energy storage device, especially high-performance supercapacitor.

2. Experimental Section

2.1. Materials

Ti_3AlC_2 MAX phase (99 %, Sigma Aldrich), HF (48 %, Thermo Fisher Scientific, India Pvt.) and HCl (37 %, Thermo Fisher Scientific), H_2SO_4 (98 %, Thermo Fisher Scientific), ethanol (CH_3CH_2OH) (99.7%, Sigma Aldrich), and deionized water (DI) used for preparing all of the solutions during synthesis process. All of the materials are of analytical grade and used without any purification.

2.2. Synthesis of MXene ($Ti_3C_2T_x$)

The $Ti_3C_2T_x$ MXene was synthesized using the Ti_3AlC_2 MAX phase by chemical etching using hydrofluoric acid (HF). First, 6 mL of deionized (DI) water, 12 mL HCl, and 2 mL of HF were combined in Teflon tube and agitated at 355 rpm. Subsequently, 1 g Ti_3AlC_2 MAX powder gently add to the etchant solution. The HF removed Al layer by generating AlF_3, resulting to the development of multilayer $Ti_3C_2T_x$. For 24 h, the mixture was constantly mixed. Following etching, the reaction mixture was centrifuged at 5000 rpm to repeatedly wash it with DI water till the pH obtain nearly neutral. The cleansed $Ti_3C_2T_x$ suspension was then mixed with 1 g of LiCl and agitated in a three-neck flask at 60 °C for two hours [25]. The delamination of MXene layers was made easier by this intercalation stage shown in **Fig. 1**. Following intercalation, the product was again purified by several centrifugation cycles at 5000 rpm to remove remaining salts and acids. Finally, the resulting $Ti_3C_2T_x$ MXene powder was dry in a vacuum oven at 80 °C for overnight.

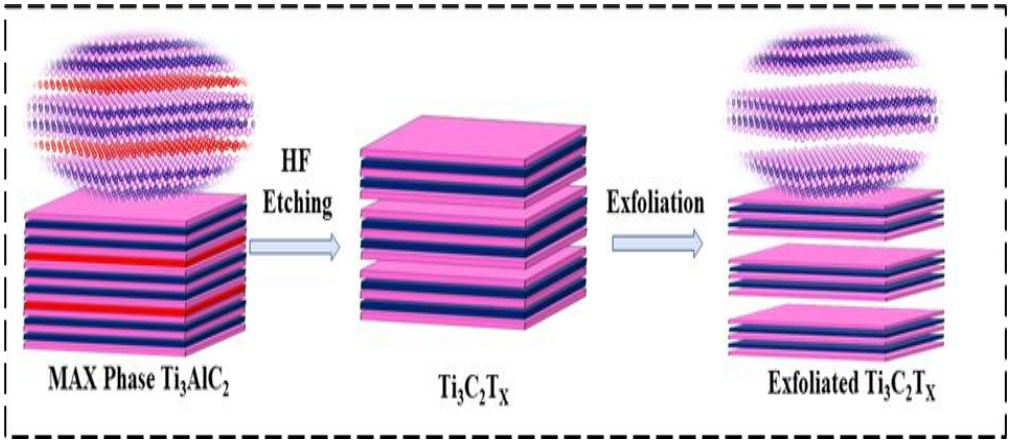

Figure 1. Graphic demonstration of synthesis of $Ti_3C_2T_x$ MXene nanosheets

2.3.Characterization

X-ray diffraction (XRD) measurement using Rigaku MiniFlex 600 diffraction were used to investigate crystallographic structure of the prepared material. Optical analysis is done by UV absorption spectra. Scanning electron microscopy (SEM; Zeiss EVO40) was used to examine the surfaces morphology of $Ti_3C_2T_x$ and by using TEM/HRTEM (JEOL 2100F,

200 kV), the morphology was thoroughly investigated, providing complete insights of interlayer spacing, morphological characteristics, and crystalline framework.

2.4. Electrochemical Measurements

The electrochemical measurements of $Ti_3C_2T_x$ MXene nanosheets was performed using Metrohm Autolab potentiostat/galvanostat (PGSTAT204) in a three-electrode setup in 1 M H_2SO_4 electrolyte. The working electrodes were the synthesized nanomaterials, and the reference and counter electrodes are Ag/AgCl and Platinum wire, respectively. The working electrode were fabricated by coating slurry having 80% $Ti_3C_2T_x$ MXene, 10% carbon black, and 10% PVDF as binder in NMP onto the nickel foam substrate and was dry for 12 hrs at 70 °C in vacuum oven. Charge storage behavior, rate capability, and interfacial kinetics were studied by cyclic voltammetry (CV), galvanostatic charge-discharge (GCD), and electrochemical impedance spectroscopy (EIS). GCD tests was performed for 1-3 A g^{-1} current densities within the potential window established by CV analysis, and CV was conducted scan rate of 20-100 mV s^{-1}. The identical electrochemical setup was used to record EIS spectra throughout a frequency range of 0.01-10^5 Hz.

3. Result and Discussion

3.1. Structural and UV-Visible absorption analysis

The crystal structure of $Ti_3C_2T_x$ MXene nanosheets was investigated by X-ray diffraction (XRD) demonstrated in **Fig. 2(a)**. The spectra of $Ti_3C_2T_x$ MXene sheets having a strong peak at angle 6.97°, 14.95°, 27.66°, 35.03°, 41.21°, 57.75° and 61.11° corresponding to the planes (002), (004), (006), (101), (105), (109) and (110), which confirms the successfully synthesis of $Ti_3C_2T_x$ MXene [26]. The removal of Al using HF acid etching process results in wide interplanar spacing, the d-spacing corresponding to the plane (002) is 1.16 nm. The crystallite size of $Ti_3C_2T_x$ MXene was found to be 13.21 nm, observed by Debye-Scherrer formula.

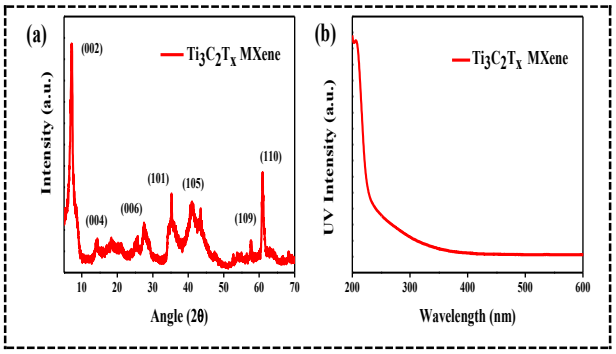

Figure. 2. (a) XRD pattern, (b) UV absorption spectra of $Ti_3C_2T_x$ MXene.

The optical properties were investigated by analyzing the UV absorption spectra of $Ti_3C_2T_x$ MXene nanosheets. As seen in **Fig. 2(b)**, the $Ti_3C_2T_x$ MXene nanosheets absorbance borders extend into the visible spectrum, with maximal absorbance points of around 208 nm. Furthermore, the Tauc plot has been used to measure the optical bandgap power of $Ti_3C_2T_x$ MXene nanosheets, which have intrinsic linear bandgaps of 1.24 eV [27].

3.2. Scanning electron microscopic (SEM) and Transmission electron microscopic (TEM) analysis

The SEM image of $Ti_3C_2T_x$ MXene nanosheets is demonstrated in **Fig. 3(a)**, which offers important morphological insights and reveals their distinctive layered shape. The residual van der Waals interactions between neighboring $Ti_3C_2T_x$ layers are responsible for the observed stacked sheet-like architecture. The TEM image of $Ti_3C_2T_x$ MXene at a scale of 100 nm is presented in

Fig. 3(b), which further supports the material's ultrathin sheet-like shape. Additionally, the HR-TEM image of $Ti_3C_2T_x$ MXene at resolution (5 nm) is shown in **Fig. 3(c)**. It clearly shows discrete lattice fringes having interlayer spacing of 1.12 nm, which is indicative of the well-defined crystalline structure [25,28].

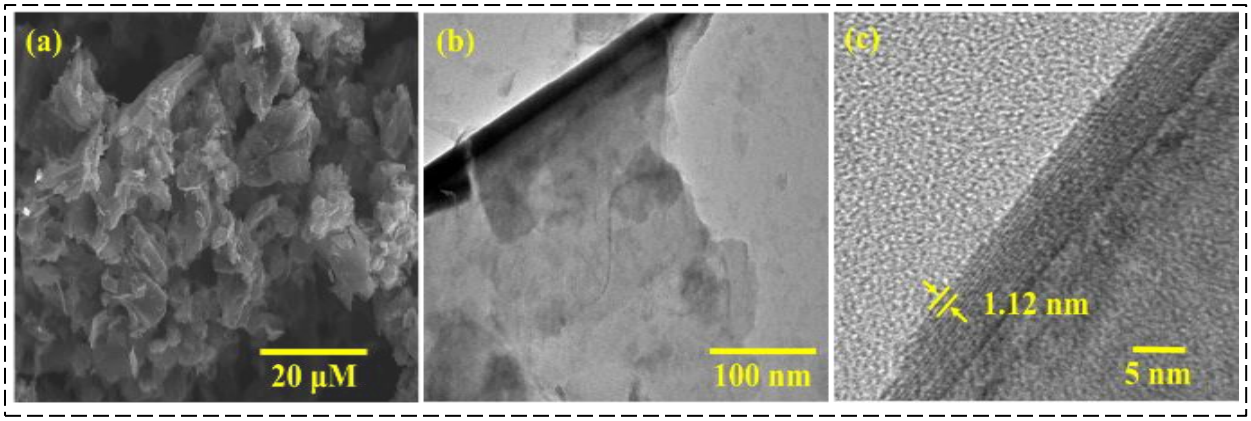

Figure 3. (a) SEM image of $Ti_3C_2T_x$ MXene, (b) TEM image of $Ti_3C_2T_x$ MXene nanosheets, (c) HR-TEM image of $Ti_3C_2T_x$ MXene nanosheets.

Electrochemical Measurements

Cyclic voltammetry (CV) and Galvanostatic charge-discharge (GCD) was used to systematically measure the electrochemical measurement of $Ti_3C_2T_x$ MXene. $Ti_3C_2T_x$ MXene nanosheets were used as the working substance, Pt wire as counter electrode, and Ag/AgCl electrode as reference electrode in a three-electrode setup for electrochemical measurements. Every measurement was performed in a potential range of -0.12 to -0.32 V in a 1 M H_2SO_4 acidic electrolyte. The following formula was used to determine the electrode's specific capacitance (C_{sp}): m is the mass of the working substance coated on nickel foam; k is scanning speed varying from (20–100 mV s^{-1}); ΔV is the potential span of (0.2 V); and ∫ Idv is the integrated area under the CV curve[29].

$$C_s = \frac{\int \mathrm{Idv}}{mk\Delta V} \quad (1)$$

The CV profile of $Ti_3C_2T_x$ MXene nanosheets is presented in **Fig. 4(a)**, and computed

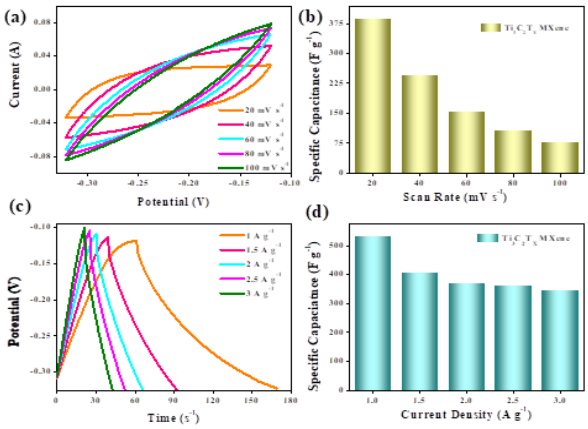

Figure 4. (a) CV measurements of Ti3C2Tx MXene, (b) Comparison bar chart of the CV specific capacitance values for

$Ti_3C_2T_x$ MXene nanosheets were 387.5, 244.24, 155.32, 105.74, and 77 F g^{-1}, at scan rate 20, 40, 60, 80, and 100 mV s^{-1}. Because

of restricted ion diffusion and decreased electrolyte accessibility at high scan rates,

Table 1: Comparison of the electrochemical behaviour of $Ti_3C_2T_x$ MXene based Supercapacitor.

Working Electrode	Electrolyte	Specific Capacitance	Current Density	Ref.
$Ti_3C_2T_x$ Powder	1 M H_2SO_4	363 F g^{-1}	1 A g^{-1}	30
$Ti_3C_2T_x$/rGO	2 M KOH	154 F g^{-1}	2 A g^{-1}	31
$Ti_3C_2T_x$/rGO	1 M H_2SO_4	357 F g^{-1}	1 A g^{-1}	25
N-doped $Ti_3C_2T_x$	6 M KOH	327 F g^{-1}	1 A g^{-1}	32
Water@ $Ti_3C_2T_x$	1 M H_2SO_4	507 F g^{-1}	1 A g^{-1}	27
GO/ $Ti_3C_2T_x$	6 M KOH	405 F g^{-1}	1 A g^{-1}	33
$Ti_3C_2T_x$	1 M H_2SO_4	535 F g^{-1}	1 A g^{-1}	This Work

specific capacity gradually decreases as scan rate increases. The $Ti_3C_2T_x$ MXene electrode's specific capacitance as a function of scan rate is demonstrated in **Fig. 4(b)** Additionally, the specific capacity of the $Ti_3C_2T_x$ MXene electrode was assessed using galvanostatic charge-discharge (GCD) experiments at numerous current densities between 1 and 3 A g^{-1} within the potential span of −0.12 to −0.32 V (vs. Ag/AgCl electrode). The GCD profiles of the $Ti_3C_2T_x$ MXene electrode recorded at various current densities are seen in **Fig. 4(c)**. These profiles show almost symmetric charge-discharge curves, which are suggestive of good capacitive performance and electrochemical reversibility [27].

$$C_s = \frac{I_m \Delta t}{\Delta V} \qquad (2)$$

The above formula was used to get the specific capacity (C_{sp}) of the three-electrode system: C_{sp} is the specific capacity, I_m is applied current density, Δt is discharging time, and ΔV is the potential span. The computed specific capacity of $Ti_3C_2T_x$ MXene were 535, 405, 370, 362.5, and 345 F g^{-1} at current densities of 1, 1.5, 2, 2.5, and 3 A g^{-1} respectively. The fast speed of ions at higher current density is the reason for the decrease in specific capacitance. The $Ti_3C_2T_x$ MXene electrode's rate capability is demonstrated in **Fig. 4(d)**, which demonstrates the specific capacity as a function of current density. The Comparison of the electrochemical behavior of $Ti_3C_2T_x$ MXene based electrode materials for supercapacitor have shown in **Table 1.**

In 1 M H_2SO_4 electrolyte, $Ti_3C_2T_x$ sheets exhibits capacitive charge storage governed by fast, reversible H^+ intercalation/deintercalation within its interlayer corridors along with surface oxidation-reduction reactions of Ti positions. The plentiful –O, –OH, and –F functional groups facilitate strong interaction with H^+ ions, while the high electrical conductivity supports rapid electron movement. Additionally, the layered structure with engorged interlayer spacing encourages efficient ion diffusion and accessibility of active sites. This synergistic mechanism outcomes in high capacitance and rate capability.

3.3. Electrochemical impedance spectroscopy (EIS)

The impedance characteristics and charge storage behavior of $Ti_3C_2T_x$ MXene nanosheets were examined using electrochemical impedance spectroscopy (EIS) throughout a frequency span of 0.01 Hz to 10^5 Hz. **Fig. 5** shows the $Ti_3C_2T_x$ MXene Nyquist plot (red curve). The EIS spectrum shows a roughly linear trend in the low-frequency values and a noticeable semicircular arc in the high-frequency values. The semicircle's shape and size offer important information on the ion transport kinetics and interfacial electrochemical reactions taking place at the electrode–electrolyte interface, while its diameter

correlates to charge-transfer resistance (R_{ct}) [28].

The electrochemical properties of the system are further clarified by the fitted curve (black curve in Fig. 5). The intrinsic resistance of the electrolyte, represented by the solution resistance (R_s), was found to be 0.83 Ω. In the meantime, it was determined that the electrode–electrolyte interface's charge-transfer resistance (R_{ct}) was 3.14 Ω, indicating effective charge transfer kinetics. Additionally, the $Ti_3C_2T_x$ MXene electrode's dominating capacitive nature and advantageous ion transport features are confirmed by the linear behavior shown in the low-frequency zone.

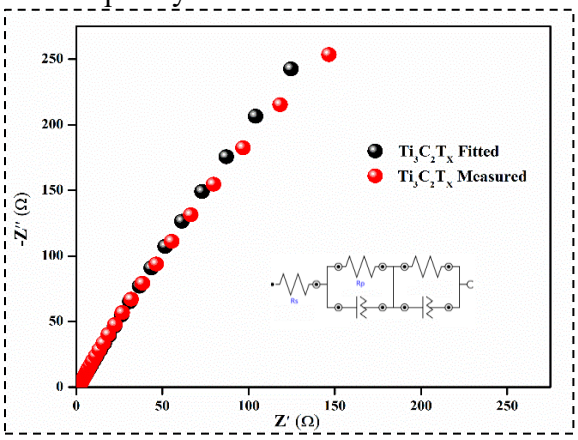

Figure. 5. Nyquist measured and fitted curves of $Ti_3C_2T_x$ MXene.

4. Conclusion

This study shows that, $Ti_3C_2T_x$ MXene nanosheets was successfully synthesized through HF etching and delamination, yielding a 2D layered structure. Structural and morphological analyses using XRD, SEM, and TEM validate the formation of few-layer $Ti_3C_2T_x$ MXene sheets with prolonged interlayer spacing, while UV–Visible spectroscopy confirmed its optical features. Electrochemical measurements in a 3-electrode setup on nickel foam demonstrated outstanding capacitive performance, attaining a large specific capacitance of 535 F g^{-1} at 1 A g^{-1}. The CV and GCD results revealed fast charge storage ability, while EIS analysis showed low R_{ct} (3.14 Ω) and efficient charge movement. The enhanced electrochemical behaviour is mainly attributed to the high electrical conductivity, available superficial area, and fast ion transport pathways within the $Ti_3C_2T_x$ MXene nanosheets. Overall, these findings reveal $Ti_3C_2T_x$ MXene as a highly promising material for electrode in revolutionary high-performance supercapacitors.

Acknowledgements

M. Singh expresses gratitude to CSIR, New Delhi, India for providing financial support in the shape of the CSIR-JRF fellowship. For financing support under project ANRF/PAIR/2025/000029/PAIR-A, we are deeply grateful to the Anusandhan National Research Foundation (ANRF), Department of Science and Technology (DST), Government of India. The authors further thank the Central Instrumentation Facility (CIF), School of Physical Sciences (SPS), Jawaharlal Nehru University (JNU), and the Advanced Instrumentation Research Facility (AIRF), JNU, for providing access to sophisticated characterization instruments.

References

(1) Zhu, Q.; Li, J.; Simon, P.; Xu, B. Two-Dimensional MXenes for Electrochemical Capacitor Applications: Progress, Challenges and Perspectives. *Energy Storage Materials* **2021**, *35*, 630–660. https://doi.org/10.1016/j.ensm.2020.11.035.

(2) Tian, Z.; Sun, Z.; Shao, Y.; Gao, L.; Huang, R.; Shao, Y.; Kaner, R. B.; Sun, J. Ultrafast Rechargeable Zn Micro-Batteries Endowing a Wearable Solar

Charging System with High Overall Efficiency. *Energy Environ. Sci.* **2021**, *14* (3), 1602–1611. https://doi.org/10.1039/D0EE03623D.

(3) Kim, H.-K.; Kamali, A. R.; Roh, K. C.; Kim, K.-B.; Fray, D. J. Dual Coexisting Interconnected Graphene Nanostructures for High Performance Supercapacitor Applications. *Energy Environ. Sci.* **2016**, *9* (7), 2249–2256. https://doi.org/10.1039/C6EE00815A.

(4) Rani, D.; Dubey, A.; Kumar, B.; Singh, M.; Sharma, A. L.; Hussain, A. M. P.; Singh, K.; Kumar, P. Hydration-Engineered Widely Interlayered Vanadium Oxide Nanobelts for High-Performance Aqueous Zinc-Ion Batteries. *Batteries & Supercaps* **2026**, *9* (5), e70300. https://doi.org/10.1002/batt.70300.

(5) Lang, X.; Hirata, A.; Fujita, T.; Chen, M. Nanoporous Metal/Oxide Hybrid Electrodes for Electrochemical Supercapacitors. *Nature Nanotech* **2011**, *6* (4), 232–236. https://doi.org/10.1038/nnano.2011.13.

(6) Sengottaiyan, C.; Kalam, N. A.; Jayavel, R.; Shrestha, R. G.; Subramani, T.; Sankar, S.; Hill, J. P.; Shrestha, L. K.; Ariga, K. BiVO4/RGO Hybrid Nanostructure for High Performance Electrochemical Supercapacitor. *Journal of Solid State Chemistry* **2019**, *269*, 409–418. https://doi.org/10.1016/j.jssc.2018.10.011.

(7) Kim, Y.; Park, T.; Na, J.; Yi, J. W.; Kim, J.; Kim, M.; Bando, Y.; Yamauchi, Y.; Lin, J. Layered Transition Metal Dichalcogenide/Carbon Nanocomposites for Electrochemical Energy Storage and Conversion Applications. *Nanoscale* **2020**, *12* (16), 8608–8625. https://doi.org/10.1039/D0NR01664K.

(8) Simon, P.; Gogotsi, Y.; Dunn, B. Where Do Batteries End and Supercapacitors Begin? *Science* **2014**, *343* (6176), 1210–1211. https://doi.org/10.1126/science.1249625.

(9) Yang, P.; Mai, W. Flexible Solid-State Electrochemical Supercapacitors. *Nano Energy* **2014**, *8*, 274–290. https://doi.org/10.1016/j.nanoen.2014.05.022.

(10) Kumar, P.; Srivastava, P.; Singh, J.; Belwal, R.; Pandey, M. K.; Hui, K. S.; Hui, K. N.; Singh, K. Morphological Evolution and Structural Characterization of Bismuth Telluride (Bi_2 Te_3) Nanostructures. *J. Phys. D: Appl. Phys.* **2013**, *46* (28), 285301. https://doi.org/10.1088/0022-3727/46/28/285301.

(11) Pumera, M. Graphene-Based Nanomaterials and Their Electrochemistry. *Chem. Soc. Rev.* **2010**, *39* (11), 4146. https://doi.org/10.1039/c002690p.

(12) Liu, C.; Yu, Z.; Neff, D.; Zhamu, A.; Jang, B. Z. Graphene-Based Supercapacitor with an Ultrahigh Energy Density. *Nano Lett.* **2010**, *10* (12), 4863–4868. https://doi.org/10.1021/nl102661q.

(13) Mansourpanah, Y. MXenes and Other 2D Nanosheets for Modification of Polyamide Thin Film Nanocomposite Membranes for Desalination. *Separation and Purification Technology* **2022**, *289*, 120777. https://doi.org/10.1016/j.seppur.2022.120777.

(14) Kim, S.; Wang, H.; Lee, Y. M. 2D Nanosheets and Their Composite Membranes for Water, Gas, and Ion Separation. *Angewandte Chemie* **2019**, *131* (49), 17674–17689. https://doi.org/10.1002/ange.201814349.

(15) Prasad, J.; Singh, A. K.; Tomar, M.; Gupta, V.; Singh, K. Hydrothermal Synthesis of Micro-Flower like Morphology Aluminum-Doped MoS2/rGO Nanohybrids for High Efficient Electromagnetic Wave Shielding Materials. *Ceramics International* **2021**, *47* (11), 15648–15660. https://doi.org/10.1016/j.ceramint.2021.02.135.

(16) Lukatskaya, M. R.; Kota, S.; Lin, Z.; Zhao, M.-Q.; Shpigel, N.; Levi, M. D.; Halim, J.; Taberna, P.-L.; Barsoum, M. W.; Simon, P.; Gogotsi, Y. Ultra-High-Rate Pseudocapacitive Energy Storage in Two-Dimensional Transition Metal Carbides. *Nat Energy* **2017**, *2* (8), 17105. https://doi.org/10.1038/nenergy.2017.105.

(17) Anasori, B.; Lukatskaya, M. R.; Gogotsi, Y. 2D Metal Carbides and Nitrides (MXenes) for Energy Storage. *Nat Rev Mater* **2017**, *2* (2), 16098. https://doi.org/10.1038/natrevmats.2016.98.

(18) Hussain, S.; Vikraman, D.; Ali Sheikh, Z.; Taqi Mehran, M.; Shahzad, F.; Mujasam Batoo, K.; Kim, H.-S.; Kim, D.-K.; Ali, M.; Jung, J. WS2-Embedded MXene/GO Hybrid Nanosheets as Electrodes for Asymmetric Supercapacitors and Hydrogen Evolution Reactions. *Chemical Engineering Journal* **2023**, *452*, 139523. https://doi.org/10.1016/j.cej.2022.139523.

(19) Shekhirev, M.; Shuck, C. E.; Sarycheva, A.; Gogotsi, Y. Characterization of MXenes at Every Step, from Their Precursors to Single Flakes and Assembled Films. *Progress in Materials Science* **2021**, *120*, 100757. https://doi.org/10.1016/j.pmatsci.2020.100757.

(20) VahidMohammadi, A.; Mojtabavi, M.; Caffrey, N. M.; Wanunu, M.; Beidaghi, M. Assembling 2D MXenes into Highly Stable Pseudocapacitive Electrodes with High Power and Energy Densities. *Advanced Materials* **2019**, *31* (8), 1806931. https://doi.org/10.1002/adma.201806931.

(21) Kshetri, T.; Tran, D. T.; Le, H. T.; Nguyen, D. C.; Hoa, H. V.; Kim, N. H.; Lee, J. H. Recent Advances in MXene-Based Nanocomposites for Electrochemical Energy Storage Applications. *Progress in Materials Science* **2021**, *117*, 100733. https://doi.org/10.1016/j.pmatsci.2020.100733.

(22) Xu, X.; Yang, L.; Zheng, W.; Zhang, H.; Wu, F.; Tian, Z.; Zhang, P.; Sun, Z. MXenes with Applications in Supercapacitors and Secondary Batteries: A Comprehensive Review. *Materials Reports: Energy* **2022**, *2* (1), 100080. https://doi.org/10.1016/j.matre.2022.100080.

(23) Priyanka; Rundla, A.; Singh, M.; Kumar, B.; Mishra, V.; Singh, K. Hierarchically Structured $CsPbBr_3$ @$Ti_3C_2T_X$ Nanohybrid Frameworks for High-Performance Supercapacitors. *ACS Appl. Energy Mater.* **2026**, *9* (6), 3038–3052. https://doi.org/10.1021/acsaem.5c03596.

(24) Xu, S.; Wei, G.; Li, J.; Han, W.; Gogotsi, Y. Flexible MXene–Graphene Electrodes with High Volumetric Capacitance for Integrated Co-Cathode Energy Conversion/Storage Devices. *J. Mater. Chem. A* **2017**, *5* (33), 17442–17451. https://doi.org/10.1039/C7TA05721K.

(25) Rundla, A.; Priyanka; Kumar, B.; Tripathi, P.; Kumar, P.; Singh, K.

Ti3C2Tx MXene@rGO Composite Electrodes for High-Performance Supercapacitor Applications. *Journal of Power Sources* **2025**, *632*, 236408. https://doi.org/10.1016/j.jpowsour.2025.236408.

(26) Priyanka; Rundla, A.; Kumar, B.; Singh, M.; Rani, D.; Kumar, P.; Mishra, V.; Singh, K. Interfacial Engineering of $Ti_3C_2T_x$ -Protected $CsPbBr_3$ Perovskite Quantum Dots for Enhanced Charge Transport and Superior Hydrogen Evolution Catalysis. *Advanced Sustainable Systems* **2026**, *10* (4), e01283. https://doi.org/10.1002/adsu.202501283.

(27) Kumar, B.; Rundla, A.; Priyanka; Singh, M.; Rani, D.; Kumar, P.; Singh, K. Synergistic Ti3C2Tx MXene Quantum Dot/Nanosheet Hybrid: Elevating Supercapacitor Performance. *Journal of Power Sources* **2025**, *652*, 237603. https://doi.org/10.1016/j.jpowsour.2025.237603.

(28) De, S.; Acharya, S.; Maity, C. K.; Nayak, G. C. Boron Nitride/$Ti_3C_2T_x$ MXene Nanosheet/WS_2 Nanostructure Ternary Composites for All-Solid-State Flexible Asymmetric Supercapacitors. *ACS Appl. Nano Mater.* **2023**, *6* (13), 11175–11186. https://doi.org/10.1021/acsanm.3c01202.

(29) Singh, M.; Kumar, B.; Rundla, A.; Priyanka; Rani, D.; Kumar, P.; Singh, K. High-Performance 1T-WS2/rGO Composites with Enhanced Charge Storage Mechanism for Supercapacitor Applications. *Journal of Energy Storage* **2025**, *140*, 118945. https://doi.org/10.1016/j.est.2025.118945.

(30) Shen, L.; Zhou, X.; Zhang, X.; Zhang, Y.; Liu, Y.; Wang, W.; Si, W.; Dong, X. Carbon-Intercalated $Ti_3C_2T_x$ MXene for High-Performance Electrochemical Energy Storage. *J. Mater. Chem. A* **2018**, *6* (46), 23513–23520. https://doi.org/10.1039/C8TA09600G.

(31) Zhao, C.; Wang, Q.; Zhang, H.; Passerini, S.; Qian, X. Two-Dimensional Titanium Carbide/RGO Composite for High-Performance Supercapacitors. *ACS Appl. Mater. Interfaces* **2016**, *8* (24), 15661–15667. https://doi.org/10.1021/acsami.6b04767.

(32) Yoon, Y.; Lee, M.; Kim, S. K.; Bae, G.; Song, W.; Myung, S.; Lim, J.; Lee, S. S.; Zyung, T.; An, K. A Strategy for Synthesis of Carbon Nitride Induced Chemically Doped 2D MXene for High-Performance Supercapacitor Electrodes. *Advanced Energy Materials* **2018**, *8* (15), 1703173. https://doi.org/10.1002/aenm.201703173.

(33) Xu, S.; Wei, G.; Li, J.; Han, W.; Gogotsi, Y. Flexible MXene–Graphene Electrodes with High Volumetric Capacitance for Integrated Co-Cathode Energy Conversion/Storage Devices. *J. Mater. Chem. A* **2017**, *5* (33), 17442–17451. https://doi.org/10.1039/C7TA05721K.